

Excitation spectra of harmonic quantum dot lattices with Coulomb interaction between the dots and the broken generalized Kohn theorem

M. Taut*

Institute for Solid State and Materials Research Dresden, POB 270016, 01171 Dresden, Germany

(Received 31 August 2000; published 1 March 2001)

Lattices of parabolic quantum dots with different dot species per unit cell and Coulomb interaction between the dots are investigated. As examples, we solve the Schrödinger equation for square lattices with two different dots per unit cell: (i) two different circular dots, and (ii) two elliptical dots, which are rotated by 90° relative to each other. The interaction between the dots is considered in a dipole approximation, and excitation spectra are calculated. For *vanishing* momentum transfer ($\mathbf{q}=0$), the energy spectrum of the first case can be expressed as a superposition of two noninteracting dots with an effective confinement frequency, which includes the effect of dot interaction. Only in the second case is there a splitting of degenerate absorption lines, and an anticrossing occurs, which is a qualitative indication of interdot interaction. If the interaction becomes very strong and if all lattice sites (not necessarily confinement potentials) are equivalent, then the contribution of the dot interaction outweighs possible differences in the confinement potentials and the generalized Kohn theorem gradually reenters, in the sense that one pair of excitation modes (pseudo-Kohn modes) becomes independent of the interaction strength. For *finite* momentum transfer ($\mathbf{q}\neq 0$), we investigated mode softening and the influence of changing the interaction strength between dots of different sublattices. The latter effect may be implemented by putting different electron numbers in different dot species. It is shown that strengthening the next-nearest-neighbor interaction versus the nearest-neighbor interaction stabilizes the square lattice.

DOI: 10.1103/PhysRevB.63.115319

PACS number(s): 73.21.-b, 73.20.Mf

I. INTRODUCTION

Quantum dots are frequently called “artificial atoms,” and small interacting quantum dot arrays “artificial molecules.” There are numerous exact (and approximate) calculations of these. “Artificial solids” are more complicated to handle, because brute force calculations are not possible here. We applied the dipole approximation for the interdot interaction and neglected overlap between the dots, which is justified in the van der Waals limit. The Schrödinger equation for harmonic confinement potentials, and with a homogeneous magnetic field perpendicular to the plane, can then be solved exactly. The generalized Kohn theorem¹ (GKTh) plays a crucial role in quantum dot physics with far-reaching consequences. It considers interacting electron systems in a harmonic confinement and a constant magnetic field, and it states that excitations by long-wavelength radiation are not affected by the electron-electron (ee) interaction. This statement applies to arrays of *identical* harmonic dot confinements (with ee interaction between the dots) as well (see the Appendix of Ref. 2). This does not mean that all excitations are independent of ee interaction, but only optically active ones (Kohn modes), and it does not mean that ee interaction is not important for other excitations. However, this fact prevents the ee interaction from being seen and investigated, e.g., by far infrared (FIR) spectroscopy. The FIR absorption spectrum of the whole system agrees exactly with the spectrum of a single particle. The GKTh does not hold for arrays of *different* dot confinements, e.g., periodic dot lattices with two different harmonic dot confinements per unit cell.² Then all collective modes are excited by FIR radiation and affected by ee interaction, or, in other words, there is no Kohn mode. The calculation and investigation of absorption fre-

quencies and probabilities in the latter case is the subject of this work.

In order to obtain a visual picture, let us first consider a classical model for the Kohn mode for a vanishing magnetic field. (This preliminary consideration will be replaced by a rigorous quantum-mechanical treatment in the following.) Classically, the charge distributions of all dots oscillate rigidly in phase with the bare confinement frequency, and the ee interaction contributes only a constant term to the total energy (independent of elongation). If we have more than one *identical* dot per unit cell, there are additional collective modes, in which the individual dots oscillate out of phase, and which are affected by dot interaction, but which are not optically active. Consequently, the dot interaction is not observable with FIR spectroscopy in arrangements of *identical* dots. One way to trick Kohn’s theorem is to include *different* dot species. Then there is no coherent oscillation mode for all dots, which does not change the ee interaction energy of the system in elongation, because there is no common bare confinement frequency. As a consequence, all collective modes (two modes per dot in the unit cell) are affected by dot interaction and excited by FIR radiation with a finite probability. In other words, the generalized Kohn theorem for dot arrays is broken. Other systems where Kohn’s theorem does not hold comprise (i) anharmonic confinements^{3,5} (circular dots with r^4 and higher-order terms in the radial dependence or square dots with terms of type x^2y^2), and (ii) hole dots with different effective masses.⁶ One point of this paper is that the GKTh can be broken *despite* an exactly harmonic Hamiltonian. A further possibility for observing the ee interaction in the excitations is to consider a finite wavelength,^{2,3} which is also considered in the present work. The most interesting issue in this case is mode softening due

to dot interaction, and how it can be controlled.

In Sec. II we discuss the magnetophonon Hamiltonian used here. In Sec. III the eigensolutions including excitation spectra are found. Section IV is devoted to a calculation of the oscillator strength for FIR absorption, and in Sec. V analytical and numerical results for $\mathbf{q}=0$ and $\mathbf{q}\neq 0$ are given. Sec. VI is a summary. A preliminary paper of the results for $\mathbf{q}=0$ has been published elsewhere.⁴

II. MAGNETOPHONON HAMILTONIAN

The first part of the calculation of the eigenstates of the Hamiltonian closely follows the procedure described in Ref. 2. We have only to consider that *now the confinement potentials and electron numbers can be different* in different dots. After introducing center-of-mass (c.m.) and relative coordinates in each dot, and, applying the dipole approximation for the Coulomb interaction between the dots, do we observe that the Hamiltonian of all c.m. coordinates is decoupled from individual dot Hamiltonians in the relative coordinates. That is why all excitations can be classified into (i) collective (c.m.) excitations, and (ii) intradot excitations. The latter are not considered here because they are not optically active. The Hamiltonian in the c.m. coordinates $\mathbf{R}_{n,\alpha}$ reads, in atomic units $\hbar=m=e=1$ (also see Sec. IV A in Ref. 2),

$$H_{c.m.} = \sum_{n,\alpha} \frac{1}{2m^*} \left[\frac{\mathbf{P}_{n,\alpha}}{\sqrt{N_\alpha}} + \frac{\sqrt{N_\alpha}}{c} \mathbf{A}(\mathbf{U}_{n,\alpha}) \right]^2 + \frac{1}{2} \sum_{\substack{n,\alpha \\ n',\alpha'}} \sqrt{N_\alpha N_{\alpha'}} \mathbf{U}_{n,\alpha} \cdot \mathbf{C}_{n,\alpha;n',\alpha'} \cdot \mathbf{U}_{n',\alpha'}, \quad (1)$$

where $\mathbf{U}_{n,\alpha} = \mathbf{R}_{n,\alpha} - \mathbf{R}_{n,\alpha}^{(0)}$ is the elongation of the c.m. at lattice site (n, α) and $\mathbf{P}_{n,\alpha} = -i\nabla_{\mathbf{U}_{n,\alpha}}$ is the corresponding canonical momentum operator. n runs over the unit cells, and α over the dot species within a cell. N_α is the number of electrons in dot α , and m^* the effective mass. It is clear already from inspection of Eq. (1) that the eigenvalues of $H_{c.m.}$ do not depend on the explicitly shown electron numbers N_α , because the factors $\sqrt{N_\alpha}$ can be considered just as a rescaling factor of the coordinates $\mathbf{U}_{n,\alpha}$. However, the eigenfunctions (and quantities derived from them) do depend on the explicit N_α . The force-constant tensor reads

$$C_{n,\alpha;n,\alpha} = \mathbf{\Omega}_\alpha + \epsilon^{-1} N_\alpha \sum_{n',\alpha' (\neq n,\alpha)} \mathbf{T}(\mathbf{R}_{n,\alpha}^{(0)} - \mathbf{R}_{n',\alpha'}^{(0)}) \quad (2)$$

$$C_{n,\alpha;n',\alpha'} = -\epsilon^{-1} \sqrt{N_\alpha N_{\alpha'}} \mathbf{T}(\mathbf{R}_{n,\alpha}^{(0)} - \mathbf{R}_{n',\alpha'}^{(0)}) \quad \text{for} \\ (n, \alpha) \neq (n', \alpha'), \quad (3)$$

where ϵ^{-1} is the inverse background dielectric constant and $\mathbf{\Omega}_\alpha$ the bare confinement tensor, which produces a harmonic confinement. The dipole tensor is defined as $\mathbf{T}(\mathbf{a}) = 1/a^5 [3\mathbf{a}\mathbf{a} - a^2\mathbf{I}]$, where (\circ) denotes the dyad product and \mathbf{I} the unit tensor. Observe that \mathbf{C} depends on N_α implicitly, which affects the energy eigenvalues.

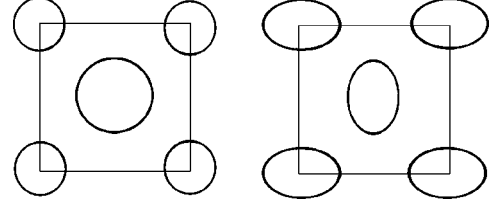


FIG. 1. Minimum unit cells for the two dot architectures considered in this paper, with two different circular dots (left) and two identical, but rotated, ellipsoidal dots (right).

A unitary transformation to collective magnetophonon coordinates

$$\mathbf{U}_{n,\alpha} = \frac{1}{\sqrt{N_c}} \sum_{\mathbf{q}}^{BZ} e^{-i\mathbf{q}\cdot\mathbf{R}_n^{(0)}} \mathbf{U}_{\mathbf{q},\alpha} \quad (4)$$

$$\mathbf{P}_{n,\alpha} = \frac{1}{\sqrt{N_c}} \sum_{\mathbf{q}}^{BZ} e^{+i\mathbf{q}\cdot\mathbf{R}_n^{(0)}} \mathbf{P}_{\mathbf{q},\alpha}, \quad (5)$$

where N_c is the number of unit cells, leaves us with a sum on N_c decoupled subsystems $H_{c.m.} = \sum_{\mathbf{q}} H_{\mathbf{q}}$,

$$H_{\mathbf{q}} = \sum_{\alpha} \frac{1}{2m^*} \left[\frac{\mathbf{P}_{\mathbf{q},\alpha}}{\sqrt{N_\alpha}} + \frac{\sqrt{N_\alpha}}{c} \mathbf{A}(\mathbf{U}_{\mathbf{q},\alpha}^*) \right]^\dagger \cdot \left[\frac{\mathbf{P}_{\mathbf{q},\alpha}}{\sqrt{N_\alpha}} + \frac{\sqrt{N_\alpha}}{c} \right. \\ \left. \times \mathbf{A}(\mathbf{U}_{\mathbf{q},\alpha}^*) \right] + \frac{1}{2} \sum_{\alpha,\alpha'} \sqrt{N_\alpha N_{\alpha'}} \mathbf{U}_{\mathbf{q},\alpha}^* \cdot \mathbf{C}_{\mathbf{q};\alpha,\alpha'} \cdot \mathbf{U}_{\mathbf{q},\alpha'}, \quad (6)$$

which includes the dynamical matrix

$$\mathbf{C}_{\mathbf{q};\alpha,\alpha'} = \sum_n e^{i\mathbf{q}\cdot\mathbf{R}_n^{(0)}} \mathbf{C}_{\alpha,\alpha'}(\mathbf{R}_n^{(0)}), \quad \mathbf{C}_{\alpha,\alpha'}(\mathbf{R}_n^{(0)}) = \mathbf{C}_{n,\alpha;0,\alpha'}. \quad (7)$$

With Eqs. (2) and (3), we obtain

$$\mathbf{C}_{\mathbf{q};\alpha,\alpha} = \mathbf{\Omega}_\alpha + \epsilon^{-1} N_\alpha \sum_{\alpha' (\neq \alpha)} \mathbf{T}(\mathbf{a}_\alpha - \mathbf{a}_{\alpha'}) \\ + \sum_{n \neq 0} \left[\sum_{\alpha'} \mathbf{T}(\mathbf{R}_n^{(0)} + \mathbf{a}_\alpha - \mathbf{a}_{\alpha'}) - e^{i\mathbf{q}\cdot\mathbf{R}_n^{(0)}} \mathbf{T}(\mathbf{R}_n^{(0)}) \right], \quad (8)$$

$$\mathbf{C}_{\mathbf{q};\alpha,\alpha'} = -\epsilon^{-1} \sqrt{N_\alpha N_{\alpha'}} \sum_n e^{i\mathbf{q}\cdot\mathbf{R}_n^{(0)}} \\ \times \mathbf{T}(\mathbf{R}_n^{(0)} + \mathbf{a}_\alpha - \mathbf{a}_{\alpha'}) \quad \text{for } \alpha \neq \alpha', \quad (9)$$

where $\mathbf{R}_{n,\alpha}^{(0)} = \mathbf{R}_n^{(0)} + \mathbf{a}_\alpha$, and $n \neq 0$ under the sum means that the term $\mathbf{R}_n^{(0)} = 0$ is excluded.

Now we consider a simple square lattice, alternatively occupied by two different dot species. The minimum unit cell is face centered square (see Fig. 1) with lattice constant a . For long-wavelength modes (the index $\mathbf{q}=0$ is dropped henceforth) and after performing the lattice sum involved in Eq. (7) numerically, we obtain the four 2×2 dynamical matrices

$$\mathbf{C}_{11} = \boldsymbol{\Omega}_1 + dp_1 \mathbf{I}, \quad (10)$$

$$\mathbf{C}_{22} = \boldsymbol{\Omega}_2 + dp_2 \mathbf{I}, \quad (11)$$

$$\mathbf{C}_{12} = \mathbf{C}_{21} = -dp_{12} \mathbf{I}, \quad (12)$$

with $d = 1.460$ and the interaction parameters

$$p_i = 2N_i \epsilon^{-1}/a^3 \quad (i=1,2), \quad (13)$$

$$p_{12} = 2\sqrt{N_1 N_2} \epsilon^{-1}/(a/\sqrt{2})^3 = p. \quad (14)$$

The dynamical matrix for $\mathbf{q} \neq 0$ is more complicated, and is not given explicitly.

III. EIGENSTATES

Now we are going to find the eigenvalues and eigenfunction of Eq. (6). For avoiding divergences for $B=0$, we add an isotropic oscillator potential $\frac{1}{2} \sum_{\alpha} \omega_0^2 \mathbf{U}_{\alpha}^2$ to the kinetic energy in Eq. (6), and subtract it from the interaction term. ω_0 is in principle arbitrary, but we chose the mean value of the bare confinement frequencies included in $\boldsymbol{\Omega}_1$ and $\boldsymbol{\Omega}_2$. Now we replace the coordinates in Eq. (6) (for $\mathbf{q}=0$) by boson ladder operators. This is analogous to the usual textbook transformation (see, e.g., Ref. 7, Sec. 3.3) apart from the factors $\sqrt{N_{\alpha}}$. It is obvious that this modification can be taken into account by introducing scaled coordinates $\mathbf{U}_{\alpha} \rightarrow \tilde{\mathbf{U}}_{\alpha} = \sqrt{N_{\alpha}} \mathbf{U}_{\alpha}$ (which implies $\mathbf{P}_{\alpha} \rightarrow \tilde{\mathbf{P}}_{\alpha} = \mathbf{P}_{\alpha}/\sqrt{N_{\alpha}}$),

$$\sqrt{N_{\alpha}} U_{\alpha x} = \frac{1}{2} \sqrt{\frac{2}{\tilde{\omega}_c^*}} (a_{\alpha 1}^+ + a_{\alpha 2}^+ + a_{\alpha 1} + a_{\alpha 2}), \quad (15)$$

$$\sqrt{N_{\alpha}} U_{\alpha y} = -\frac{i}{2} \sqrt{\frac{2}{\tilde{\omega}_c^*}} (a_{\alpha 1}^+ - a_{\alpha 2}^+ - a_{\alpha 1} + a_{\alpha 2}), \quad (16)$$

where the first subscript ($\alpha=1,2$) indicates the dot number and the second the component. The transformation of the c.m. momentum operators is analogous:

$$\frac{P_{\alpha x}}{\sqrt{N_{\alpha}}} = \frac{i}{2} \sqrt{\frac{\tilde{\omega}_c^*}{2}} (a_{\alpha 1}^+ + a_{\alpha 2}^+ - a_{\alpha 1} - a_{\alpha 2}), \quad (17)$$

$$\frac{P_{\alpha y}}{\sqrt{N_{\alpha}}} = \frac{1}{2} \sqrt{\frac{\tilde{\omega}_c^*}{2}} (a_{\alpha 1}^+ - a_{\alpha 2}^+ + a_{\alpha 1} - a_{\alpha 2}). \quad (18)$$

The cyclotron frequency is $\omega_c^* = B/m^*c$ and $\tilde{\omega}_c^* = \sqrt{\omega_c^{*2} + 4\omega_0^2}$. First, it is clear that the Hamiltonian in these ladder operators no longer shows an explicit N_{α} dependence (apart from that implicit in the dynamical matrix). This implies that the eigenvalues of the Hamiltonian do not depend on those N_{α} , which are seen explicitly in Eq. (6). Second, the commutators of the ladder operators are not influenced by the N_{α} factors, and agree with those of bosons: $[a_{\alpha i}, a_{\alpha i}^+] = 1$, and all other commutators vanish.⁸ (This is because the commutators of $\tilde{\mathbf{U}}_{\alpha}$ and $\tilde{\mathbf{P}}_{\alpha}$ agree with the commutators of

the untilded quantities.) Now the total Hamiltonian can be written in matrix notation in the compact form

$$H = [\mathbf{a}^+ \mathbf{a}] \cdot \mathbf{H} \cdot \begin{bmatrix} \mathbf{a} \\ \mathbf{a}^+ \end{bmatrix}, \quad (19)$$

where

$$[\mathbf{a}^+ \mathbf{a}] = [a_{11}^+ a_{12}^+ a_{21}^+ a_{22}^+ | a_{11} a_{12} a_{21} a_{22}], \quad (20)$$

and $[\mathbf{a}^+]$ is the transposed and Hermitian conjugate of Eq. (21). The 8×8 Hamiltonian matrix is not unique, but can be cast into the form

$$\mathbf{H} = \begin{bmatrix} \alpha & \beta \\ \beta^* & \alpha^* \end{bmatrix} \quad \text{with} \quad \alpha^+ = \alpha, \quad \beta^T = \beta \quad (21)$$

consisting of the 4×4 matrices

$$\alpha = \frac{1}{2} \begin{bmatrix} \omega & 0 \\ 0 & \omega \end{bmatrix} + \frac{1}{4\tilde{\omega}_c^*} \mathbf{E}^+ \cdot \begin{bmatrix} \tilde{\mathbf{C}}_{11} & \mathbf{C}_{12} \\ \mathbf{C}_{21} & \tilde{\mathbf{C}}_{22} \end{bmatrix} \cdot \mathbf{E}, \quad (22)$$

$$\beta = \frac{1}{4\tilde{\omega}_c^*} \mathbf{E}^+ \cdot \begin{bmatrix} \tilde{\mathbf{C}}_{11} & \mathbf{C}_{12} \\ \mathbf{C}_{21} & \tilde{\mathbf{C}}_{22} \end{bmatrix} \cdot \mathbf{E}^*, \quad (23)$$

with $\mathbf{E} = \begin{bmatrix} \varepsilon & 0 \\ 0 & \varepsilon \end{bmatrix}$ and the 2×2 matrices

$$\tilde{\mathbf{C}}_{kk} = \mathbf{C}_{kk} - \frac{1}{2} \omega_0^2 \mathbf{I}, \quad \omega = \begin{bmatrix} \omega_+ & 0 \\ 0 & \omega_- \end{bmatrix}, \quad \varepsilon = \begin{bmatrix} 1 & 1 \\ i & -i \end{bmatrix}, \quad (24)$$

with

$$\omega_{\pm} = \sqrt{\omega_o^2 + \left(\frac{\omega_c^*}{2}\right)^2} \pm \left(\frac{\omega_c^*}{2}\right). \quad (25)$$

Finding the eigenstates of the boson Hamiltonian [Eq. (19)] is provided by mathematical physics, and described in Ref. 9 in full detail. The goal is to find a linear transformation $[\mathbf{b}^+] = \mathbf{A} \cdot [\mathbf{a}^+]$, which preserves boson commutators and diagonalizes H . We shall only summarize the recipe here.

The *eigenvalues* are given by $E_{n_1, n_2, n_3, n_4} = \sum_k^{(1, \dots, 4)} (n_k + \frac{1}{2}) \omega_k$ with n_k being non-negative integers and $\omega_k = 2\gamma_k$ with γ_k being the four *positive* eigenvalues of the matrix $\mathbf{H} \cdot \mathbf{J}$. The 8×8 matrix $\mathbf{J} = \begin{bmatrix} \mathbf{1} & \mathbf{0} \\ \mathbf{0} & -\mathbf{1} \end{bmatrix}$ is made up of 4×4 unit matrices. All eigenvalues of $\mathbf{H} \cdot \mathbf{J}$ come in pairs $(\gamma_k, -\gamma_k)$.

The *eigenfunctions* of H are constructed as usual for bosons:

$$|n_1, n_2, n_3, n_4\rangle = \prod_k^{(1, \dots, 4)} \frac{(b_k^+)^{n_k}}{\sqrt{n_k!}} |0\rangle. \quad (26)$$

The four eigenvectors belonging to the positive eigenvalues are written in the form $\mathbf{x}_k = \begin{bmatrix} u_k \\ v_k \end{bmatrix}$. The column vectors of \mathbf{A}^+ are given by the vectors \mathbf{x}_k , and by the vectors $\hat{\mathbf{x}}_k = \begin{bmatrix} v_k^* \\ u_k^* \end{bmatrix}$, which are the eigenvectors belonging to $-\gamma_k$. The eigenvectors have to be properly orthonormalized $\mathbf{x}_i^+ \cdot \mathbf{J} \cdot \mathbf{x}_k = \delta_{i,k}$. Without degeneracy, the orthogonality is guaranteed auto-

matically. The inverse of this particular transformation is obtained from $\mathbf{A}^{-1} = \mathbf{J} \cdot \mathbf{A}^+ \cdot \mathbf{J}$, which shows that the linear transformation is not unitary (but unitary in a non-Euclidian metric).

IV. OSCILLATOR STRENGTH

Optical oscillator strengths (for $\mathbf{q}=0$) between the states $|n\rangle = |n_1, n_2, n_3, n_4\rangle$ and $|n'\rangle = |n'_1, n'_2, n'_3, n'_4\rangle$ for polarization in the $\eta=(x \text{ or } y)$ direction are defined as

$$f_{n,n';\eta} = 2m^* \omega_{n,n'} |\langle n | \mathbf{U}_{\eta;tot} | n' \rangle|^2, \quad (27)$$

where $\omega_{n,n'}$ is the corresponding excitation energy, and $\mathbf{U}_{\eta;tot}$ is the η component of the total c.m. of the electrons in a unit cell (apart from a constant term). In formulas, this means $\mathbf{U}_{tot} = (N_1/N_{tot})\mathbf{U}_1 + (N_2/N_{tot})\mathbf{U}_2$, where $N_{tot} = N_1 + N_2$. After expressing the vectors \mathbf{U} by ladder operators b_k and b_k^+ and using Eq. (26), we obtain the usual selection rules, i.e., only one quantum with energy ω_k can be absorbed or emitted, so that we obtain only four absorption lines. The result for the oscillator strength for the four possible transitions ($k=1, \dots, 4$) and for η polarization reads

$$f_{k,\eta} = \frac{m^* \omega_k}{N_{tot} \tilde{\omega}_c^*} |S_{k,\eta}|^2 \cdot \begin{cases} (n_k + 1) \\ n_k \end{cases} \text{ for } \begin{cases} \text{absorption} \\ \text{emission}, \end{cases} \quad (28)$$

where n_k denotes the initial state, and

$$S_{k,x} = \sum_i^{(1,2)} \sqrt{\frac{N_1}{N_{tot}}} (u_{ki} - v_{ki}) + \sum_i^{(3,4)} \sqrt{\frac{N_2}{N_{tot}}} (u_{ki} - v_{ki}), \quad (29)$$

$$S_{k,y} = \sum_i^{(1,2)} \sqrt{\frac{N_1}{N_{tot}}} (-1)^{(i+1)} (u_{ki} + v_{ki}) + \sum_i^{(3,4)} \sqrt{\frac{N_2}{N_{tot}}} (-1)^{(i+1)} (u_{ki} + v_{ki}). \quad (30)$$

In the last definition, u_{ki} and v_{ki} for $i=1, \dots, 4$ are the components of the vectors \mathbf{u}_k and \mathbf{v}_k , respectively. The oscillator strength defined in Eq. (27) fulfills the following exact f -sum rule $\sum_k f_{k,\eta} = 1/N_{tot}$. It is worth pointing out that for equal electron numbers in either dot ($N_1 = N_2 = N$), the oscillator strength depends explicitly on N (contrary to the optical excitation energies). In all figures presented below the oscillator strengths are for $N_1 = N_2 = N$.

V. RESULTS

Now the two simplest cases are discussed in more detail: two different circles and two identical, but rotated, ellipses. The ratio of the two bare confinement frequencies involved in either case is 1:1.5 which means that the two confinement frequencies in units of the mean frequency ω_0 are 1.2 and 0.8. In our figures, all frequencies (energies) are given in units of the mean confinement frequency ω_0 and the interaction parameters p in units of ω_0^2 . The magnetic field is given in terms of the effective cyclotron frequency ω_c^* in units of ω_0 (upper scale) and in T (lower scale). The conversion between both scales is provided by

$$\omega_c^*[\omega_0] = \frac{0.9134 \times 10^{-2}}{m^* \omega_0 [\text{a.u.}^*]} B[\text{T}]. \quad (31)$$

In our figures we used $\omega_0 = 0.2 \text{ a.u.}^* = 2.53 \text{ meV}$ and m^* of GaAs for this conversion. (We want to stress that this parameter choice affects only the magnetic field scale and not the curves.) The definitions of the interaction parameters (13) for GaAs in more convenient units reads

$$p_i[\omega_0^2] = \frac{2.26 \times 10^7 N_i}{(a[\text{\AA}])^3 (\omega_0[\text{meV}])^2}. \quad (32)$$

(For a more detailed discussion of order-of-magnitude estimates, see Ref. 2.)

A. Zero wave number

For two different *circular dots* with bare confinement frequencies ω_1 and ω_2 and $N_1 = N_2$, the absorption spectrum and the oscillator strength are shown in Fig. 2. Although *all* absorption lines are affected by the dot interaction (represented by the interaction parameter p), and *all* modes are optically active, there is no *qualitative* effect of interaction in the position of the absorption lines. The reason for this can be understood easily. In this particular case, the four eigenmodes can be calculated analytically providing

$$\omega_{1,2,3,4} = \sqrt{\omega_{eff,i}^2 + \left(\frac{\omega_c^*}{2}\right)^2} \pm \left(\frac{\omega_c^*}{2}\right) \quad (i=1,2) \quad (33)$$

where

$$\omega_{eff,1,2}^2 = \frac{(\omega_1^2 + \omega_2^2)}{2} + \frac{(p_1 + p_2)}{2} d \pm \sqrt{\left[\frac{(\omega_1^2 + \omega_2^2)}{2} + \frac{(p_1 + p_2)}{2} d\right]^2 - (\omega_1^2 p_2 d + \omega_2^2 p_1 d + \omega_1^2 \omega_2^2)}. \quad (34)$$

(The upper and lower sign belongs to $\omega_{eff,1}$ and $\omega_{eff,2}$, respectively). Consequently, if we had to interpret an experimental spectrum, we could do this using formula (34) for noninteracting dots, but with the effective (i.e., interaction affected) confinement parameters defined into Eq. (35). Only if we take the intensities into account can we see some qualitative effect.

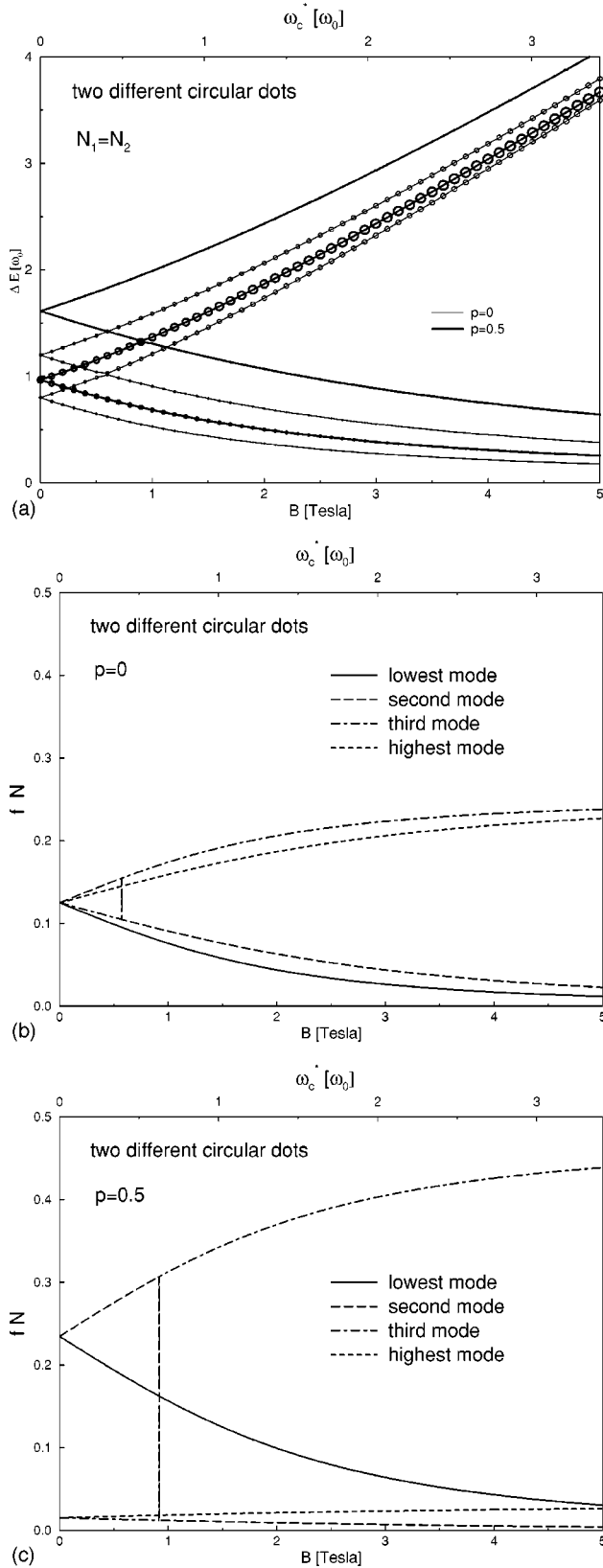


FIG. 2. Excitation modes (a) and oscillator strength (multiplied with N) for $p=0$ (b) and $p=0.5$ (c) for a lattice with two different circular dots, as described in the text. The radius of the circles in (a) is proportional to the oscillator strength, and provides a rough overview.

Whereas for noninteracting dots (with $p=0$) and for $B=0$ the oscillator strength of all modes agree (for a single oscillator, f is independent of the oscillator frequency), there is a large difference for interacting dots at $p=0.5$. This large difference can be understood as follows. In the limit $p \rightarrow \infty$, the upper pair of modes develops into a spurious Brillouin-zone boundary mode, which has a vanishing oscillator strength, and the sum rule has to be fulfilled only by the lower pair (also see the discussion below).

In Fig. 2 both dot species bare the same number of electrons. Therefore, only one interaction parameter p is involved. Calculations with different N_i (and p_i) do not show any qualitative difference. In the limit of large p (and equal electron numbers), from Eq. (34) we obtain

$$\omega_{eff,1,2}^2 = \frac{(\omega_1^2 + \omega_2^2)}{2} + \begin{cases} 2pd & \pm \frac{(\omega_1^2 - \omega_2^2)}{8pd} + O(p^{-3}). \end{cases} \quad (35)$$

Consequently, the square of the smaller effective confinement frequency (which is the only one giving rise to modes with a finite oscillator strength for large p) approaches the mean value of both squared bare confinement frequencies, whereas the larger one grows continuously for large p .

In Figs. 3 and 4(b) we show the results for two identical, but mutually rotated, *elliptical dots*. Without dot interaction ($p=0$), we have two doubly degenerate lines. With increasing interaction strength, we observe a splitting of degenerate modes and an anticrossing behavior for finite B . As in the case of circular dots, the oscillator strength at $B=0$ for noninteracting dots ($p=0$) agree for all four modes. The dot interaction lifts this degeneracy. Additionally, at $p=0.5$ we observe that the oscillator strength in the limits of small and large magnetic fields is considerable only for two of the modes, except in the gap region, where three modes contribute. By comparison of Figs. 3(a) and 4(b), we see that the magnetic field for minimum gap (between the second and third mode) increases with increasing p , whereas the gap width decreases. Consequently, the location and width of the gap provides information on the interaction strength.

By comparison of Figs. 2 and 3 with Fig. 4, and more clearly by consideration of formula (36) and Fig. 5, it becomes clear that in either case the lower pair of degenerate modes at $B=0$ converges to a constant (the mean-square bare confinement frequency $\sqrt{(\omega_1^2 + \omega_2^2)}/2$, which amounts to $1.02\omega_0$ in our numerical example). Even for finite B , there are two branches, which converge to a finite (B -dependent) value for $p \rightarrow \infty$, or, in other words, which become independent of p in this limit. At first sight this looks surprising because the ee interaction does not show any saturation, if we increase the interaction parameter, but it continues to compress the dot state. However, there is a simple visual explanation for this feature: Generally, the dot interaction adds an additional second-order contribution to the confinement, which has the same symmetry as the lattice, i.e., it is circular for a square lattice. For large p , this additional term outweighs the bare confinement, and the effective confinement in both dots becomes isotropic and equal. Thus we approach the case of a lattice of identical dots, for which a

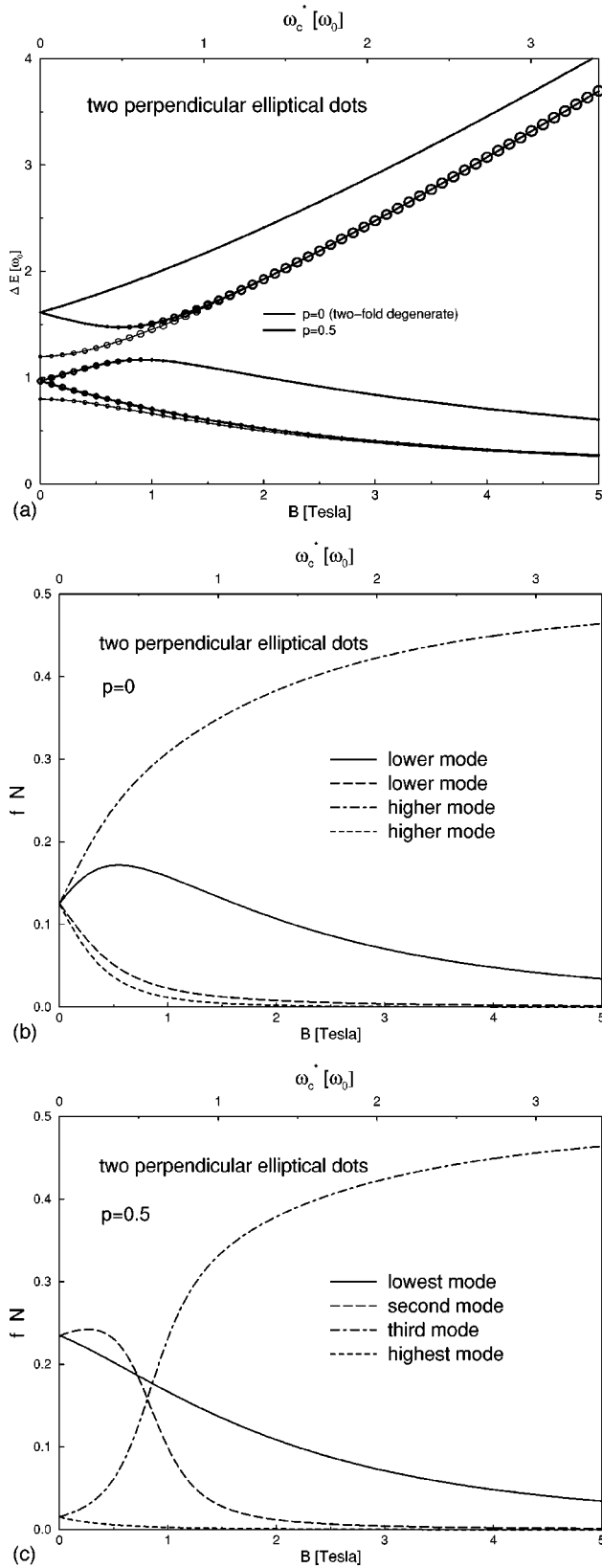


FIG. 3. Excitation modes (a) and oscillator strength (multiplied with N) for $p=0$ (b) and $p=0.5$ (c) for a lattice with two identical, but rotated, elliptical dots, as described in the text and shown in Fig. 1. The radius of the circles in (a) is proportional to the oscillator strength, and provides a rough overview.

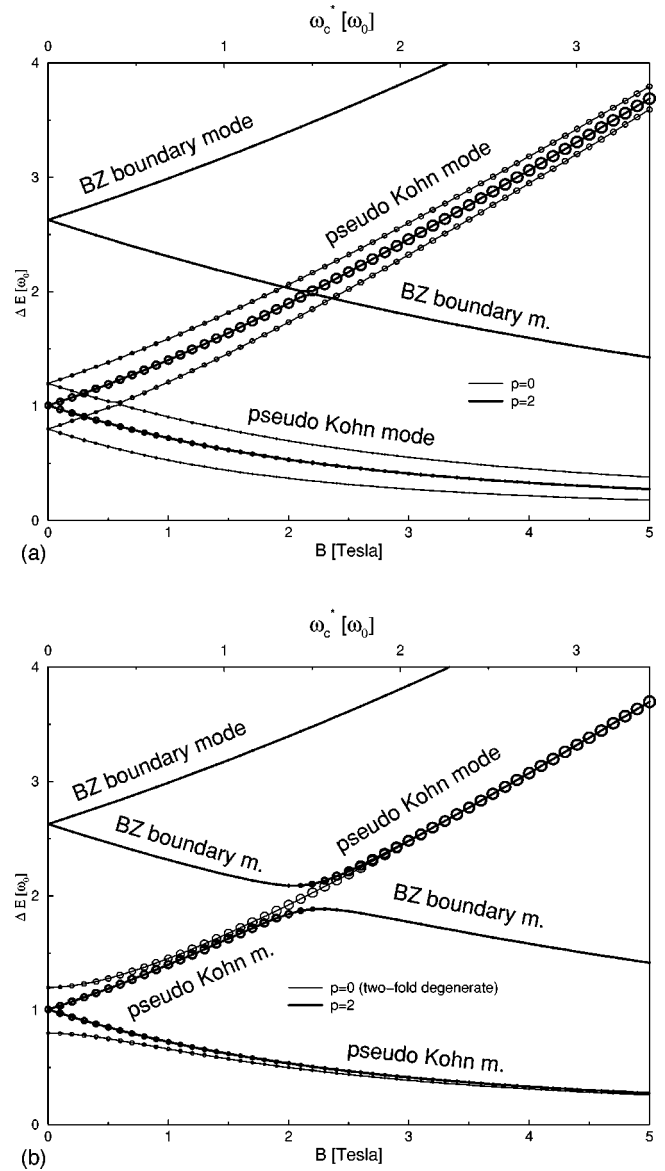


FIG. 4. Excitation modes for a lattice with two different circular dots (a) and two rotated elliptical dots (b) for a large interaction parameter ($p=2$). The radius of the circles is proportional to the corresponding oscillator strength.

pair of Kohn modes exists. Because these Kohn modes do not exactly agree with the modes of noninteracting dots, we call them *pseudo-Kohn* modes. In a sense, the generalized Kohn theorem reenters for dot lattices with strong interdot interaction. In other lattices with lower symmetry, the effective confinement in the strong-interaction limit might be elliptical, leading to pseudo-Kohn modes with a gap at $B=0$. The other pair of modes (which diverge for $p \rightarrow \infty$) turns into in-folded modes at the Brillouin-zone (BZ) corner (because the units cell halves if all dots become equivalent). These modes become spurious in the long-wavelength and large- p limits, and the oscillator strengths converge to zero.

In Figs. 3(a) and 4(b) we observe an additional qualitative effect of dot interaction. For isolated elliptical dots we ex-

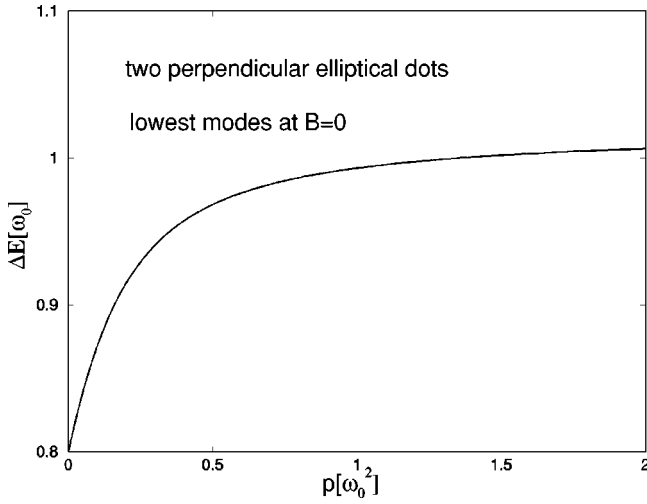


FIG. 5. Pseudo-Kohn mode at $B=0$ as a function of interaction parameter p for a lattice with two perpendicular elliptical dots per unit cell.

pect a gap between the two excitation branches at $B=0$. However, for larger p only the pseudo-Kohn mode might be observable, because the oscillator strength of the BZ boundary mode decrease rapidly. On the other hand, the two lower modes for finite p develop out of the degenerate lower mode for $p=0$, whereby the degeneracy at $B=0$ survives. Therefore, at $B=0$ it looks as if we had a circular dot. The closing of the gap between the two most intensive branches at $B=0$ is *not* a gradual effect proceeding with increasing p , but is caused by symmetry.

B. Finite wave number

In Figs. 6 and 7 the excitation energies at two symmetry points in the Brillouin zone are shown for the two lattice types shown in Fig. 1. These figures supplement Figs. 2(a) and 3(a), which belong to the center of the BZ. The most important conclusion for *circular dots* seems to be that for finite \mathbf{q} the spectrum cannot be described by effective confinement frequencies anymore (as for $\mathbf{q}=0$). Second, for small p , the crossing of the second and third modes at $\mathbf{q}=(1/2,0)$ persists, whereas it develops into an anticrossing at $\mathbf{q}=(1/2,1/2)$. For elliptical dots, dot interaction removes the degeneracy without a qualitative difference between $\mathbf{q}=(1/2,0)$ and $\mathbf{q}=(1/2,1/2)$.

In Fig. 8 we show the dispersion of the excitation energies at $B=0$ for both lattice types. In both cases the *critical* interaction parameter was chosen, where the lattice becomes unstable. One conclusion is that a lattice of circular dots is more stable than from elliptical dots. In all cases considered so far the electron numbers in either dot species agree. Now we manipulate this parameter in the case of different circular dot confinements in order to obtain additional effects. If the electron number in the shallower (larger) dot is four times that of the other one, but the interaction parameter between nearest neighbors (i.e., different dot species) is unchanged,

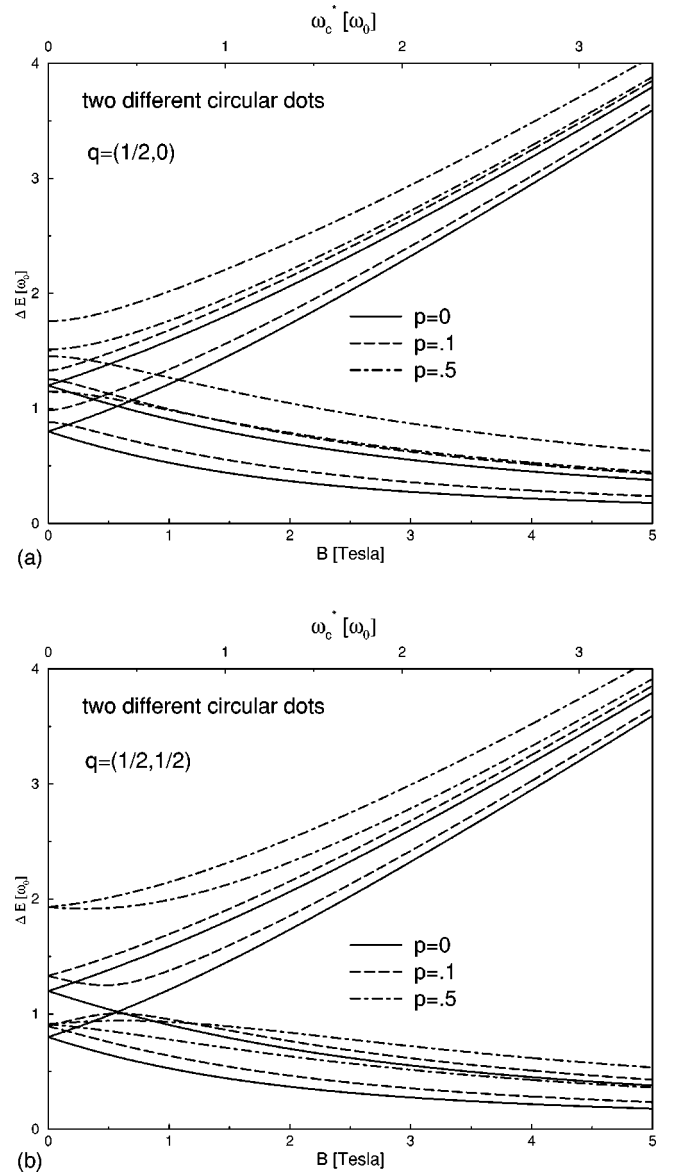


FIG. 6. Excitation modes for a lattice with two different circular dots for finite-momentum transfer on two symmetry points in the Brillouin zone: $\mathbf{q}=(1/2,0)$ (a) and $\mathbf{q}=(1/2,1/2)$ (b).

the interaction parameters defined in Eqs. (14) and (13) read $p_{12}=p=3.449$, $p_1=0.697$, and $p_2=2.439$. p_{12} refers to the interaction between the dots of different sublattices, and p_i to the interaction between dots of the same sublattices. In Fig. 8(a) these parameters are $p_{12}=p=3.449$ and $p_1=p_2=1.219$. As seen in Fig. 9, strengthening next-nearest neighbors interacting in sublattice 2 by increasing p_2 stabilizes the lattice, because the softening at $\mathbf{q}=(1/2,1/2)$ is reduced. This is easily understood. If the nearest-neighbor interaction dominates, we have virtually a simple square lattice which is electrostatically unstable. Increasing the next-nearest-neighbor interaction (at least in one sublattice) mimics an environment for one sublattice with a larger coordination number, which is more stable against deformation. A further numerical result, which is not seen in the figures, states that

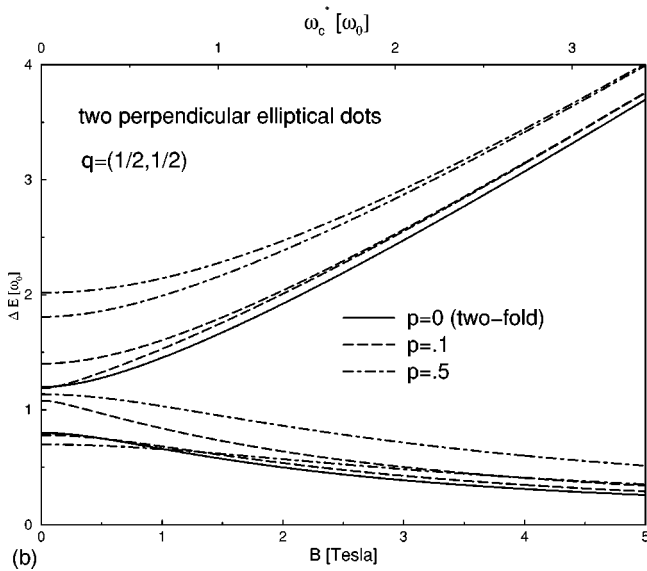
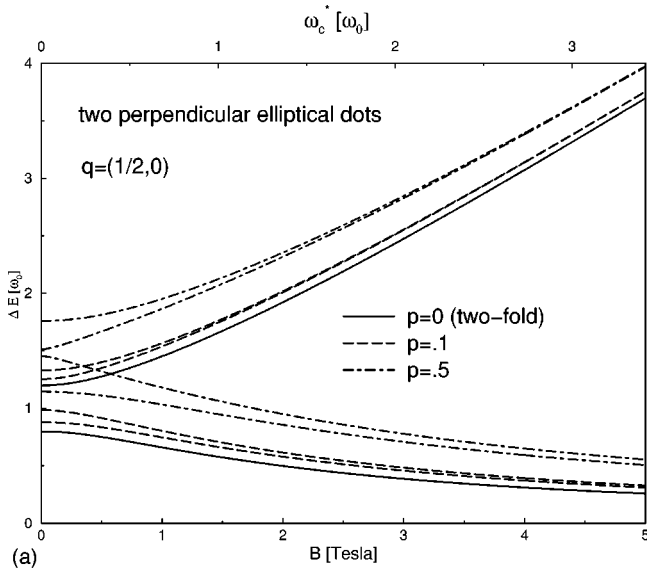


FIG. 7. Excitation modes for a lattice with two identical, but rotated, elliptical dots for finite-momentum transfer on two symmetry points in the Brillouin zone: $\mathbf{q}=(1/2,0)$ (a) and $\mathbf{q}=(1/2,1/2)$ (b).

the critical p is independent of B . This agrees with the corresponding conclusion in lattices with one dot per unit cell.²

VI. SUMMARY

We investigate harmonic dot lattices, where the generalized Kohn theorem does not hold, and we show that breaking the GKTh by constructing quantum dot lattices with at least two different dot confinements per unit cell has experimentally observable consequences.

As to *zero momentum transfer*, there are no longer any Kohn modes (interaction independent modes). In both of the considered lattice types, the degeneracy in the far-infrared intensities at $B=0$ between the upper and lower absorption lines is lifted. For two mutually rotated elliptical dots (per cell), we also observe a splitting of formerly degenerate ab-

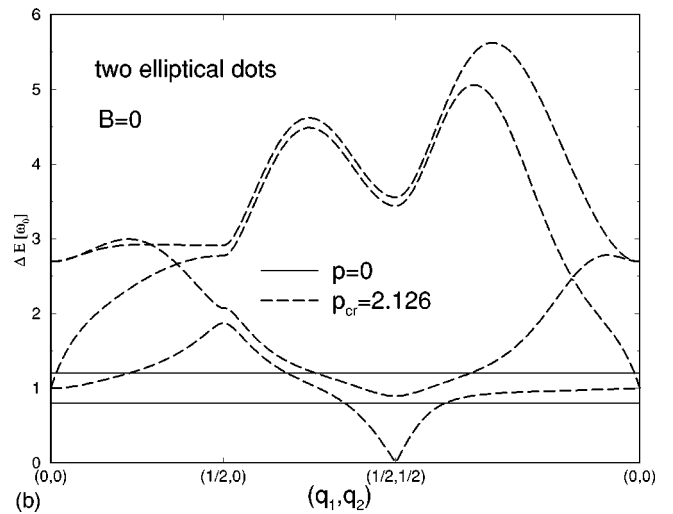
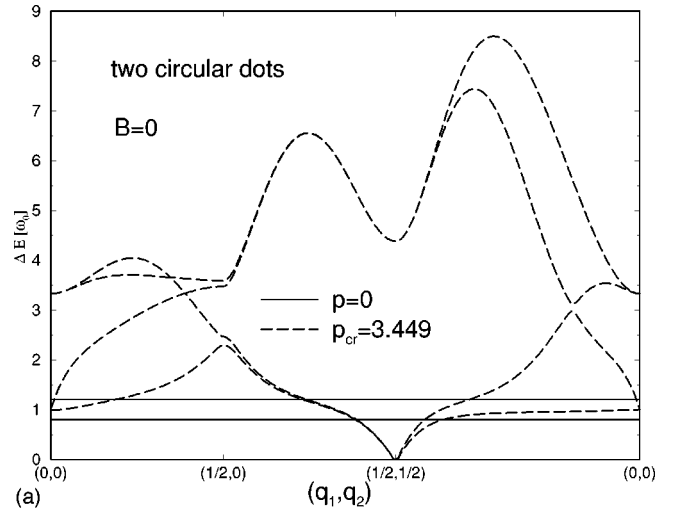


FIG. 8. Magnetophonon dispersion on the symmetry lines of the Brillouin zone for the critical interaction strength. (a) For two different circular dots. (b) For two identical, but rotated, elliptical dots per unit cell.

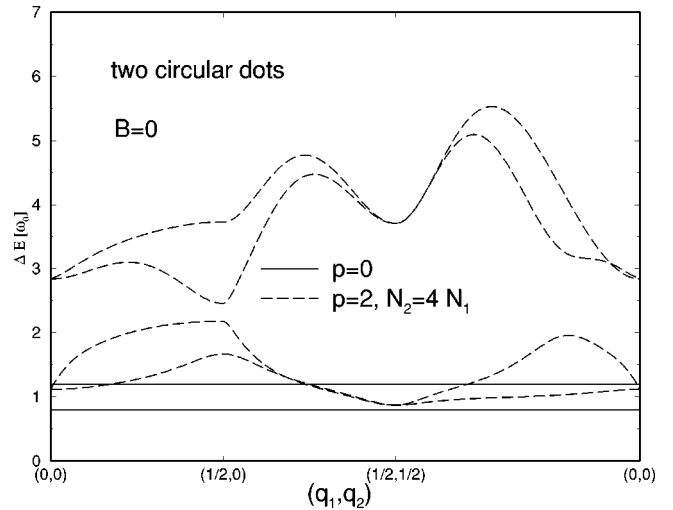


FIG. 9. As Fig. 8(a), but with different electron numbers in either dot: $N_2=4N_1$.

sorption *frequencies* and the appearance of an anticrossing due to dot interaction. For two different circular dots no qualitative effect of ee interaction in the absorption frequencies is observed. Instead, the absorption spectrum can be reproduced by two noninteracting dots with modified (effective) confinements. We also point out that an extensively strong interaction destroys the effect of interaction by producing pseudo-Kohn modes. Although this limit can hardly be reached experimentally, it might be important to take this tendency into consideration.

The excitation spectra for *finite momentum transfer* show mode softening and a lattice instability. The critical interaction strength for the instability is independent of magnetic field, but can be affected by manipulating the electron number per dot, which can change the ratio of nearest- and next-nearest-neighbor interaction strength.

Only in the case of two circular dots and $\mathbf{q}=0$ is there a simple analytical closed-form solution. However, with the formulas presented above, the absorption frequencies (and for $\mathbf{q}=0$ also the oscillator strength) for any square lattice with two harmonic dot species can be easily calculated. The only numerical task is to find the eigenvalues of an explicitly given non-Hermitian 8×8 matrix (and to perform a special sum over the eigenvector components in order to obtain the oscillator strength).

ACKNOWLEDGMENTS

I am indebted to D. Heitmann, J. Kotthaus, and H. Eschrig, and their groups, as well as G. Paasch for helpful discussions.

*Email: m.taut@ifw-dresden.de

- ¹W. Kohn, Phys. Rev. **123**, 1242 (1961); L. Brey, N. F. Johnson, and B. I. Halperin, Phys. Rev. B **40**, 10 647 (1989); P. A. Maksym and T. Chakraborty, Phys. Rev. Lett. **65**, 108 (1990); F. M. Peeters, Phys. Rev. B **42**, 1486 (1990).
- ²M. Taut, Phys. Rev. B **62**, 8126 (2000); cond-mat/0002155 (unpublished). In Phys. Rev. B **62**, formula (16) shows a misprint: the second sequence “Q=” has to be deleted in the middle of the formula (also see the correct formula in cond-mat).
- ³D. Heitmann, K. Bollweg, V. Gudmundson, T. Kurth, and S. P. Riege, Physica E **1**, 204 (1997).

⁴M. Taut, cond-mat/0007054 (unpublished).

- ⁵D. Pfannkuche and R. Gerhardts, Phys. Rev. **44**, 13 132 (1991).
- ⁶T. Darnhofer, U. Rössler, and D. A. Broido, Phys. Rev. B **52**, 14 376 (1995); **53**, 13 631 (1996).
- ⁷L. Jacak, P. Hawrylak, and A. Wojs, *Quantum Dots* (Springer, New York, 1998).
- ⁸J. Dempsey, N. F. Johnson, L. Brey, and B. I. Halperin, Phys. Rev. B **42**, 11 708 (1990).
- ⁹C. Tsallis, J. Math. Phys. **19**, 277 (1978); Y. Tikoshinsky, *ibid.* **20**, 406 (1979).